IEEE Access
Multidisciplinary | Rapid Review | Open Access Journal

Received May 30, 2018, accepted June 25, 2018, date of publication June 29, 2018, date of current version July 19, 2018.

Digital Object Identifier 10.1109/ACCESS.2018.2851572

Dynamic Inspection of Rail Wear via a Three-Step Method: Auxiliary Plane Establishment, Self-Calibration, and Projecting

CHAO WANG[1,2], HONGLI LIU[1], ZIJI MA[1], AND JIUZHEN ZENG[2]
[1]School of Electrical and Information Engineering, Hunan University, Changsha 410082, China
[2]School of Electrical Engineering, University of South China, Hengyang 421001, China

Corresponding author: Hongli Liu (honglliu@hnu.edu.cn)

This work was supported in part by the National Natural Science Foundation of China under Grant 61771191 and in part by the Natural Science Foundation of Hunan Province under Grant 2017JJ2052.

ABSTRACT Structured-light vision (SLV) is a standard approach for inspecting rail wear. However, it is incompetent for dynamic inspection due to the random vibrations in the line laser projector. In this paper, a three-step distortion rectifying method is introduced to address this issue. Given an image with two rail profile stripes, the first step involves parallelity constraint-based establishment of an auxiliary plane whose normal vector is parallel with the rail longitudinal axis. The establishment is only dependent on the intrinsic camera parameters, which improves the robustness of the auxiliary plane to the random vibrations in the line laser projector. In step two, this auxiliary plane is utilized for the autonomous calibration of the line structured lights. The proposed self-calibration is achieved by minimizing the point set mapping errors on triple matching primitives such as rail jaw, railhead inner, and rail foot and requires only two laser stripes. After these two steps, two rail profiles are reconstructed from the double-line SLV without known poses, and the distorted one is projected onto the auxiliary plane for distortion rectifying. It is able to deliver more precise rectifying than the parallel-line SLV and cross-line SLV, even if the inspecting task is performed dynamically. With the comprehensive experiments, we test our scheme and compare it with the related methods. The experimental results verify that the proposed method outperforms the previous works in terms of the accuracy and robustness for the dynamic wear inspection.

INDEX TERMS Dynamic inspection, parallelity constraint, self-calibration, line structured-light, rail wear.

I. INTRODUCTION

Nowadays, the accurate and effective track inspection is becoming a periodical and crucial task for avoiding risks and preventing accidents [1], [2]. Rail wear measurement plays a critical role in track quality inspection, whose results show the rail section geometry in a straightforward way and provide the reliable and scientific guidance for the maintenance on the track quality [3].

Structured-light vision (SLV) is a classic non-contact technique (NCT) for the rail wear inspection [4], [5], which owns a number of advantages such as flexibility, lower cost, and convenience in feature matching. SLV mainly comprises an area-array camera and a line laser projector [6], [7]. Through the calibration of the camera and projector [8], [9], the extraction of light stripeïijN̆ and the coordinate transformation from the image coordinate frame to the world coordinate frame, section wear is able to be calculated. And in general, SLV is hung from the bottom of the rail maintaining train to inspect the wear dynamically. Herein, dynamic inspection is defined as the real-time detection during train operation. While the train is moving, since SLV system and the rail are independent with each other, it is difficult to ensure the verticality between the light plane and the rail longitudinal axis (or the motion direction), especially in the vibration condition. This induces that the measured profile is stretched along the rail longitudinal axis or the transversal direction, i.e., the affine distortion is produced [10], which is the main cause for poor inspection precision in rail wear. To rectify the distorted profile and improve the accuracy, various methods have been put forward, such as orthogonal decomposition-based vibration coupling and decoupling [11], [12], non-rigid ICP registration [13], [14], affine transformation

model [10], [15], [16], measuring coordinate frame redefinition [17], and deviation rectifying using multi-line SLV [18]–[20].

Liu *et al.* [10] focus on the recognizing and rectifying for the affine rail profile. We discuss the differences between the normal profile and the affine one, and propose a valid similarity measuring scheme named point set mapping (PSM) to quantify the curve similarity on triple mapping primitives. The particle swarm optimization (PSO) is also employed for enhancing the similarity. Another method of ours [17] aims to define the most reliable measuring coordinate frame, which is achieved by estimating the Euler angles from the world coordinate frame to the defined measuring one. The distorted profile is rectified by projecting onto the plane x-y of the reliable measuring frame. Convex hull (CH) [16] is one of the affine invariant features and can be used to establish correspondences between the normal rail profile and the affine one. Then, the affine transformation parameters are estimated by use of four correspondences at least, and the profile rectifying is accomplished via affine inverse conversion. Sun *et al.* propose to inspect the rail profile via the parallel-line SLV. They obtain several parallel rail profiles and fit their circular arcs on rail waist. The intersections of each arcs are utilized to find the track longitudinal axis. The motion deviation is rectified by projecting the distorted profile onto an auxiliary plane which is perpendicular to the rail longitudinal axis. The recent work proposed in [20] puts forward a novel self-calibration technique used to calibrate the line light planes by itself. Based on the self-calibrated light planes and SLV model, three measuring rail profiles are reconstructed and projected for rectifying.

However, some shortcomings still exist in the above methods. The correspondences established via CH may suffer from the impact of the noise on the measured profile, such as the withdrawn points and missing points. The parallel-line SLV based scheme neglects the fact that the circular arcs on rail waist become ellipse arcs for the distorted profile, which will mislead the fitting of circular centers. Besides, the required parallel lights may be unavailable because of the assembling deviation. Therefore, both of the rectifying methods respectively based on CH and parallel-line SLV are imprecise. Furthermore, in previous work, PSM is only explored and used on the setup comprising a 2D laser displacement senor, which is expensive and with high-cost compared with SLV system. Last but not the least, the method of measuring coordinate frame redefinition adopts the off-line calibration which is sensitive to the vibrations caused by dynamic inspection. Although the on-line self-calibration in [20] is an innovative solution, two preconditions that three light planes are available at least and one of the light planes needs to be calibrated off-line limit its flexibility. These shortcomings motivate the work in this paper.

In this work, a three-step method including auxiliary plane establishment, self-calibration and projecting is studied for the rail wear dynamic inspection using the double-line SLV. Compared with the previous work in [10], this method is explored and used on the cheaper SLV system. Furthermore, the presented self-calibration is more robust than that employed in [17] with respect to the vibrations caused by dynamic inspection. Our contributions are summarized below.

1) An artful approach of fitting the rail longitudinal axis and establishing the auxiliary plane whose normal vector is parallel with the rail longitudinal axis is developed. In this step, the intrinsic camera parameters are required only, which improves the robustness of our fitting and establishing to the random vibrations in the line laser projector.
2) Utilizing the auxiliary plane, a thorough self-calibration of the multi-line structured-light is explored to autonomously calculate the light plane parameters in real time. It requires only two laser stripes and is able to free from the two preconditions mentioned above, superior to the self-calibration in [20]. The core idea of this step is to minimize the PSM differences between a projecting profile and standard one.
3) On basis of the thorough self-calibration, we propose to intersect the rail utilizing the double-line SLV without known poses, which is greater than the parallel-line SLV [18] and cross-line SLV [21], [22] in terms of the robustness to assembling deviation and pose variation. In step three, the profile projecting is implemented for distortion rectifying.

The remainder of this paper is organized as follows. Section II briefly describes double-line SLV model. Section III presents our method in detail. Section IV provides the experiments. Section V reports the conclusion.

II. DOUBLE-LINE SLV MODEL

In our case, two light planes with unknown relative pose intersect the rail, and respectively form two laser stripes synchronously captured by the camera. Utilizing the recognition and extraction of the laser stripe center from real images [23], [24], the image pixel coordinates of the measured profile can be calculated. According to the SLV model shown in Fig. 1, the image pixel coordinate can be easily transformed to the corresponding one in camera coordinate frame and world coordinate frame [25], [26].

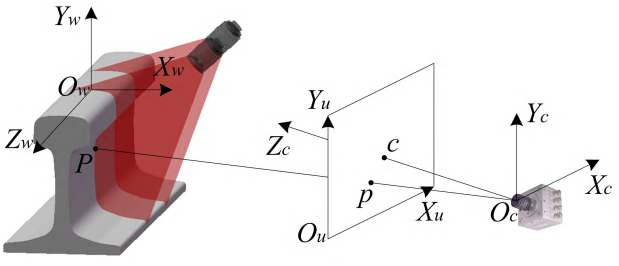

FIGURE 1. The schematic diagram of multi-line SLV with two light planes.

The transformation between a stripe point $p = (u, v)^{\mathrm{T}}$ and its corresponding point $P = (x_w, y_w, z_w)^{\mathrm{T}}$ from 3D space can

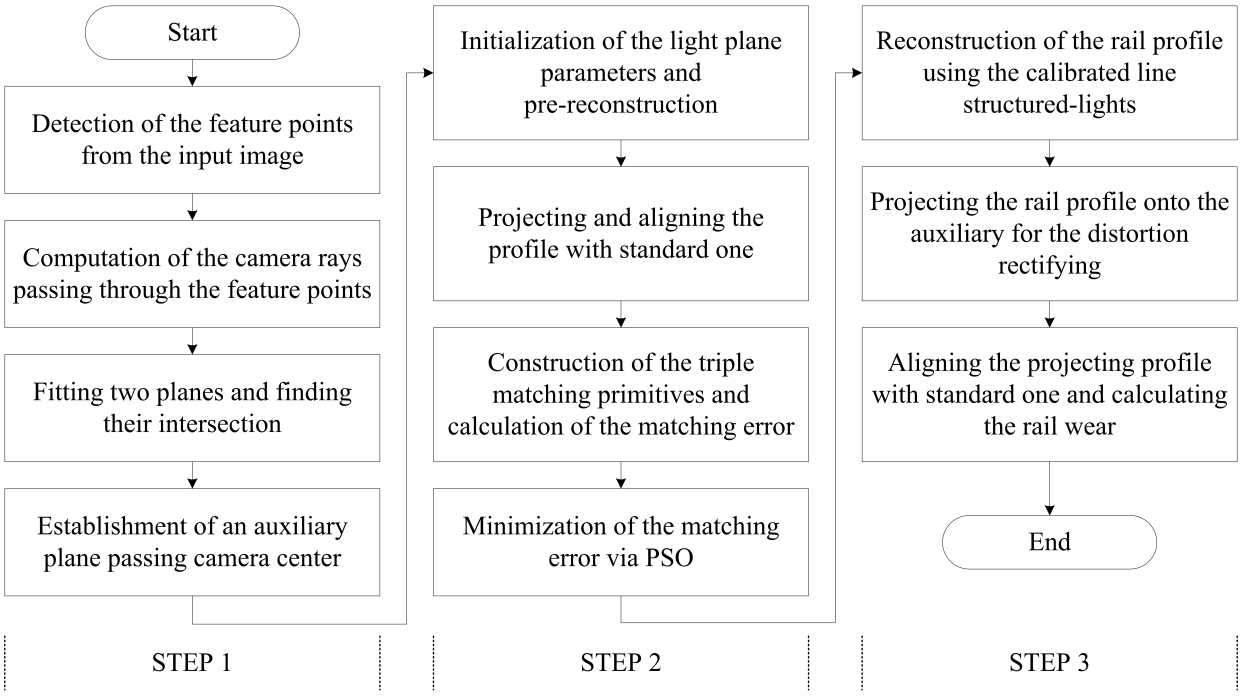

FIGURE 2. Flowchart of our three-step distortion rectifying. The first step involves parallelity constraint-based establishment of an auxiliary plane whose normal vector is parallel with the rail longitudinal axis. This plane is utilized in step two to calibrate autonomously the line structured-lights. In step three, we reconstruct the rail profile and project the distorted one onto the auxiliary plane for distortion rectifying. See text for details.

be expressed as

$$z_c \begin{bmatrix} u \\ v \\ 1 \end{bmatrix} = \boldsymbol{A}[\boldsymbol{r}_x \ \ \boldsymbol{r}_y \ \ \boldsymbol{r}_z \ \ \boldsymbol{t}] \begin{bmatrix} x_w \\ y_w \\ z_w \\ 1 \end{bmatrix} \text{ with } \boldsymbol{A} = \begin{bmatrix} f_x & \gamma & c_x \\ 0 & f_y & c_y \\ 0 & 0 & 1 \end{bmatrix} \quad (1)$$

where matrix $\boldsymbol{A}$ represents the camera intrinsic parameters, matrix $[\boldsymbol{r}_x \ \boldsymbol{r}_y \ \boldsymbol{r}_z]$ and vector $\boldsymbol{t}$ denote the camera extrinsic parameters. These parameters are calibrated offline by use of the strategy in [27]. From (1), we have

$$\begin{bmatrix} u \\ v \\ 1 \end{bmatrix} = \boldsymbol{A} \begin{bmatrix} x_c/z_c \\ y_c/z_c \\ 1 \end{bmatrix}. \quad (2)$$

Vector $[x_c/z_c, \ y_c/z_c \ , 1]^{\mathrm{T}}$ is defined as the normalized coordinates, where $(x_c, y_c, z_c)^{\mathrm{T}}$ denotes the coordinates in camera coordinate frame. Taking one of the light planes into account, its pose is expressed as

$$Ax_c + By_c + Cz_c + 1 = 0. \quad (3)$$

From (2) to (3), we have

$$\begin{cases} x_c = \dfrac{-U}{AU + BV + C} \\ y_c = \dfrac{-V}{AU + BV + C} \\ z_c = \dfrac{1}{AU + BV + C} \end{cases} \quad (4)$$

where $U = (u - c_x)/f_x$ and $V = \big(v - c_y\big)/f_y$. Parameters $(A \ B \ C)$ are the unknown variables needed to be evaluated by self-calibration.

III. THREE-STEP DISTORTION RECTIFYING

Since the dynamic inspection, there are heading and pitching vibrations [17] in the laser projector. These vibrations lead to that the laser light plane may not be perpendicular to the rail longitudinal axis. Then, the measured profile is stretched along the rail longitudinal axis or the transversal direction, i.e., the distorted profile is produced. This is the main cause for poor dynamic inspection precision in rail wear.

Provided an image containing two rail profile stripes, the proposed method aims to reconstruct the 3D rail profile and rectify the distorted one induced by heading and pitching vibrations. It involves three main steps: 1) establishment of an auxiliary plane; 2) self-calibration of line structured-lights; and 3) reconstruction and projecting, as illustrated in Fig. 2. First, we find the image coordinates of four feature points. i.e., rail jaw and rail corner via feature detection [28]. Since the intrinsic camera parameters have been calibrated beforehand, four camera rays passing through these points can be computed. Note that all the rays intersect in the camera center, and two planes can be determined from two rays respectively attached to the rail jaws and rail corners. According to the parallelity constraint, the intersecting line of these planes would be considered as the rail longitudinal axis. So, its direction vector can be employed as the normal vector of an

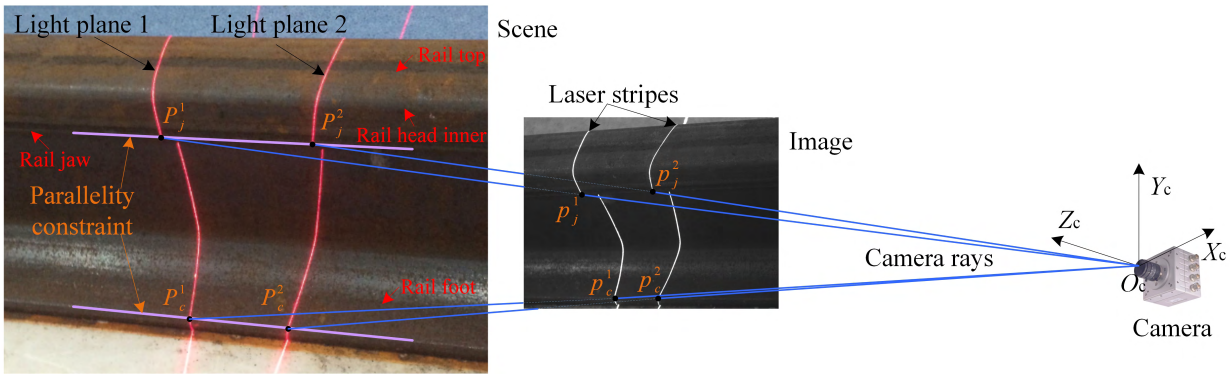

FIGURE 3. Schematic of our establishment of the auxiliary plane based on the parallelity constraint.

auxiliary plane whose normal vector is parallel with the rail longitudinal axis. Let the auxiliary plane pass through the camera center, we can uniquely establish the one we need. Next, pre-reconstruction of the rail profile is performed using the initialization of the light plane parameters and the SLV model. The 3D profile is then projected onto the auxiliary plane, yielding a projecting profile. Due to the deviation on the light plane parameters, the projecting profile would be different from the standard one in term of the size and shape. To analyze the difference quantitatively, a curve similarity measurement method is employed. As demonstrated in [10], our previously proposed PSM is highly robust and efficient. Therefore, PSM is selected as the curve similarity measurement in this paper. Based on the PSM constructed from the standard profile to the projecting one on the triple matching primitives, the self-calibration is achieved by minimizing the PSM difference via PSO. Consequently, the true rail profile can be reconstructed using the calibrated line structured-lights and projected onto the auxiliary plane for the distortion rectifying. Aligning the rectified profile with the standard one, the accurate inspection of rail wear would be achieved.

A. STEP ONE: ESTABLISHMENT OF AUXILIARY PLANE

To establish the projecting auxiliary plane, the rail longitudinal axis must be fitted. Note that it is hard to accomplish this objective from the single-line SLV [18]. That is why the double-line SLV is adopted as the gauge in our setup. As implied in [18], the direction vector of the straight line formed by several waist breakpoints can be deemed to the rail longitudinal direction. However, these points cannot be reconstructed until the corresponding light planes are calibrate correctly. Establishment of the auxiliary plane from these straight lines is infeasible for us.

In step one, a parallelity constraint-based establishment of the auxiliary plane is introduced, which requires for the intrinsic camera parameters only. The establishment is partially based on the following parallelity constraint: two parallel lines respectively located on two nonparallel planes must be parallel with the intersecting line of planes, and vice versa. In our case shown in Fig. 3, line segments $P_j^1P_j^2$ and $P_c^1P_c^2$ can be referred as the parallel lines, and triangles $\Delta P_j^1P_j^2O_c$ and $\Delta P_c^1P_c^2O_c$ would determine two nonparallel planes respectively. Herein, points P_j^i and P_c^i respectively represent the rail jaws and rail corners on light planes $i = 1, 2$, and point O_c represents the camera center. As long as we can obtain four camera rays respectively passing though points P_j^1, P_j^2, P_c^1 and P_c^2, two nonparallel planes we need would be found. Herein, the camera ray is defined as the path the light measured by every pixel travels along. By this definition, the intrinsic camera parameters essentially refer to the mapping between pixels and the associated camera rays.

In the implementation, the corner points are firstly extracted via Harris corner detection algorithm [29]. In order to pick out rail jaws and rail corners from these points, an easy solution is introduced and presented as follows. Using corner points as the center, several circles are formed with a radius of 70 pixels. If there are laser stripes both within the upper semicircle and within the lower one, the corresponding center will be identified as the rail corner. If there is one laser stripe only within the upper semicircle, the corresponding center will be identified as the rail jaw. Specifically, let $p_j^i = \left(u_j^i, v_j^i\right)$ be the pixel coordinates of the rail jaw detected from stripe i, and its associated spatial point is given by the homogeneous coordinates $P_j^i = \left(x_j^i, y_j^i, z_j^i, 1\right)^{\mathrm{T}}$. From (2) we have

$$\begin{bmatrix} x_j^i/z_j^i \\ y_j^i/z_j^i \\ 1 \end{bmatrix} = \boldsymbol{A}^{-1} \begin{bmatrix} u_j^i \\ v_j^i \\ 1 \end{bmatrix}. \tag{5}$$

Note that the equations $x_j^i/z_j^i = \boldsymbol{A}^{-1}u_j^i$ and $y_j^i/z_j^i = \boldsymbol{A}^{-1}v_j^i$ represent the parametric equations of two planes, respectively. Their solution is therefore the parametric equation of the intersecting line of these two planes, i.e., the camera ray passing through the rail jaw P_j^i. The camera rays passing through the rail foot corner P_c^i would be computed in the same way. Utilizing the camera rays, two nonparallel planes respectively passing the parallel line segments $P_j^1P_j^2$ and $P_c^1P_c^2$ can be determined. From the parallelity constraint, it is clear that the rail longitudinal axis can be referred as the intersecting

line of the two nonparallel planes. Once the fitting of rail longitudinal axis has been completed, its direction vector will be employed as the normal vector of the auxiliary plane. Since the camera center is the only one point we can determine at present, the auxiliary plane we need will be denoted as expression (6) where vector (l_x, l_y, l_z) is the direction vector of the rail longitudinal axis.

$$l_x x + l_y y + l_z z = 0. \tag{6}$$

The purpose of above efforts is to establish the most reliable auxiliary plane for the following two steps. Owing to the parallelity constraint on the feature points of different rail profiles, the proposed establishment is realized by computing four camera rays and the intersecting line, which only relies on the intrinsic camera parameters. Compared with the auxiliary plane in [18], ours owns more robustness and flexibility. In short, step one plays an important role providing the foundation for steps two and three.

B. STEP TWO: SELF-CALIBRATION OF LINE STRUCTURED-LIGHT

From (4), we learn that the equation of light plane is indispensable for the reconstructing of rail profile from single image. Essentially, the work of calibration for the line structured-light makes efforts to calculate this equation. Most of the existing methods belong to the off-line calibration which depends either on the precise template or on the correspondence from binocular vision. Unfortunately, the assembling deviation and vibrations in projector would lead to varying in the relative poses of light planes with respect to the camera [30]. That is to say, the off-line calibration is not fit to our case because of the real-time and dynamic inspection. Although the on-line self-calibration in [20] is an innovative solution, two preconditions that three light planes are available at least and one of the light planes needs to be calibrated offline limit its flexibility. Hence, an improved and thorough self-calibration is presented in this subsection.

1) PRE-ALIGNMENT OF PROJECTING PROFILE

Given the auxiliary plane obtained from step one, we first project the rail profile reconstructed by (4) onto it, and yield a projecting profile. If the parameters of the light plane used in (4) are ground-truth, the projecting profile will be same exactly with the standard one on the unworn areas. Otherwise, it would be different from the standard one in term of the size and shape. This can be utilized for the determination of the light plane parameters. In order to analyze their difference, it is needed to preliminarily align the projecting profile with the standard one. In the implementation, the double circle segment (DCS) method [10] is employed for the pre-alignment. Compared with the registration and alignment based on sparse ICP [31], our DCS owns some advantages such as simpleness and easiness which are important for the dynamic inspection. Let $P_o^{i\to p} = \left(x_o^{i\to p}, y_o^{i\to p}\right)$ and $P_o^s = \left(x_o^s, y_o^s\right)$ be the center of a circle segment from the projecting profile and its corresponding point from the standard one, respectively. There are rotation and translation operations between them, which can be given by

$$\begin{bmatrix} x_o^{i\to p} \\ y_o^{i\to p} \\ 1 \end{bmatrix}^{\mathrm{T}} = \begin{bmatrix} x_o^s \\ y_o^s \\ 1 \end{bmatrix}^{\mathrm{T}} \begin{bmatrix} \cos\theta & \sin\theta & 0 \\ -\sin\theta & \cos\theta & 0 \\ 0 & 0 & 1 \end{bmatrix} \begin{bmatrix} 1 & 0 & 0 \\ 0 & 1 & 0 \\ T_x & T_y & 1 \end{bmatrix} \tag{7}$$

where θ is the rotated angle, and T_x and T_y are the translation offsets. By fitting the centers of big and small circle segments on rail waist, DCS establishes two correspondences and estimates the transformation parameters θ, T_x and T_y. After obtaining these parameters, the projecting profile is preliminarily aligned with the standard one using expression (7). Two examples of pre-alignment are shown in Fig. 4, where projecting profiles 1 and 2 are generated with erroneous and true light plane parameters, respectively. Note that the abbreviation Dis. denotes the directional Hausdorff distance from the measured profile to the standard one.

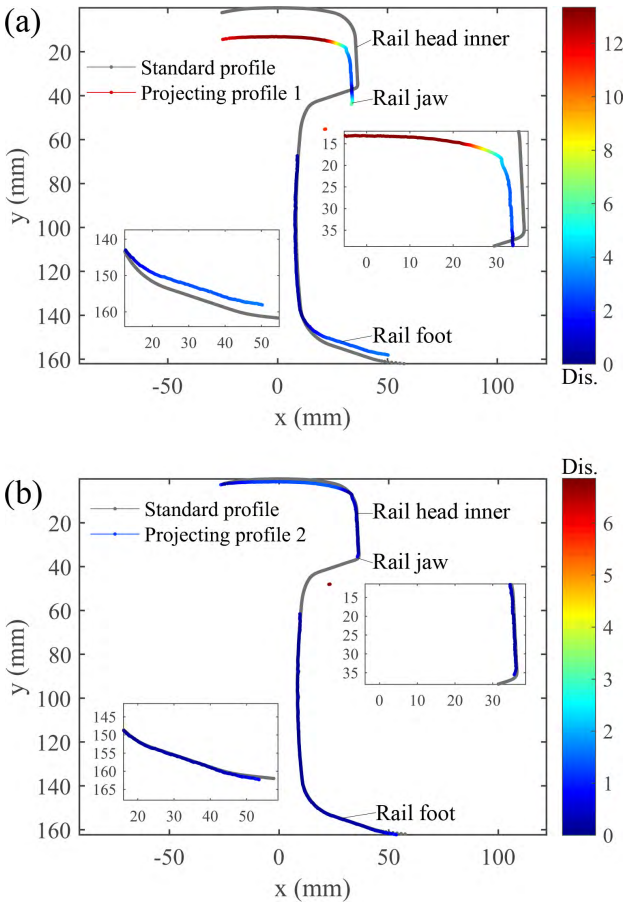

FIGURE 4. Two examples of pre-alignment for different projecting profiles. (a) The projecting profile generated with erroneous parameters. (b) The projecting profile generated with true parameters.

From the magnified version of rail jaw, rail head inner and rail foot exhibited in Fig. 4, it would be found that the projecting profile 2 matches well with the standard one on rail jaw, rail head and rail foot. On the contrary, projecting profile 1

is different from the standard one on these unworn regions, especially on the rail jaw and rail head inner. Hence, these three primitives including rail jaw, rail head inner and rail foot are selected for serving as the triple matching primitives. The quantitative errors on them are directly governed by the light plane parameters.

2) QUANTIFICATION OF MATCHING ERRORS WITH PSM

In this subsection, the quantification of the matching errors on the triple primitives is introduced. A similarity quantization method named PSM is employed in the implementation, which owns higher robustness and efficiency than the Hausdorff distance [10]. Let $P^s_{h,k} = \left(x^s_{h,k}, y^s_{h,k}\right)$ be the kth mapping point of the standard profile on rail head. Its matching error is calculated as $\left\|x^s_{h,k} - x^r_{h,k}\right\|^2$, where $x^r_{h,k}$ denotes the horizontal coordinate of the response point on the projecting profile. Then, the matching error on the rail head inner is calculated as follows

$$fitness_{\mathrm{H}} = \frac{1}{N_h}\sum_{k=1}^{N_h}\left\|x^s_{h,k} - x^r_{h,k}\right\|^2 \tag{8}$$

where N_h is the quantity of mapping points on rail head. In the same way, the mapping error on the rail foot could be denoted as

$$fitness_{\mathrm{F}} = \frac{1}{N_f}\sum_{k=1}^{N_f}\left\|x^s_{f,k} - x^r_{f,k}\right\|^2 \tag{9}$$

where N_f is the quantity of mapping points on the rail foot, coordinates $x^s_{f,k}$ and $x^r_{f,k}$ refer to the horizontal coordinate of the kth mapping point of the standard profile on rail foot and the response point on the projecting profile, respectively. Note that the rail jaw of projecting profile is a feature point which has been detected in step one. Moreover, the standard profile is referred as the rail model, which already provides the accurate location of rail jaw. The interpolation operation of PSM is therefore not required for quantification of the matching error on rail jaw. It is thus computed as expression (10), where points B^p and B^s are the rail jaw from the projecting profile and the standard one, respectively.

$$fitness_{\mathrm{B}} = \left\|B^s - B^p\right\|^2. \tag{10}$$

By observing Fig. 4(a) again, it is clear that the matching errors are mainly located on the rail head and rail jaw. Hence, the larger weight coefficient is assigned to these primitives, i.e., setting $\omega_{\mathrm{B}} = 0.5$, $\omega_{\mathrm{H}} = 0.3$ and $\omega_{\mathrm{F}} = 0.2$. The global matching error is

$$fitness = \omega_{\mathrm{H}} fitness_{\mathrm{H}} + \omega_{\mathrm{F}} fitness_{\mathrm{F}} + \omega_{\mathrm{B}} fitness_{\mathrm{B}}. \tag{11}$$

3) MINIMIZATION OF GLOBAL MATCHING ERROR

The work of self-calibration of the structured-light minimizes the global matching error via particle swarm optimization (PSO) [32], [33]. For the light plane i, we construct the position vector $\boldsymbol{X}^i_n = [A^i_n, B^i_n, C^i_n]$ $(n = 1, 2, \cdots, N)$ for each particle, and coarsely initialize the N particles by analyzing the relative pose and position between the light plane and camera. Note that the upper limit of the floating for each element is set as half of the initial value. The global matching error in (11) is acted as the fitness. In each iteration, the particle calculates the current fitness, and compares it with the previous iteration. According to the comparison, the particle records the best position and yields the best-personal and best-swarm particle denoted as $\boldsymbol{P}^i_n = [A^i_{pn}, B^i_{pn}, C^i_{pn}]^{\mathrm{T}}$ and $\boldsymbol{G}^i = [A^i_g, B^i_g, C^i_g]^{\mathrm{T}}$, respectively. On basis of the $\boldsymbol{P}^i_n$ and $\boldsymbol{G}^i$, the velocity and position are updated iteratively for the optimization of the swarm. These procedures could be expressed as

$$\boldsymbol{V}^{i,k+1}_n = \omega \boldsymbol{V}^{i,k}_n + c_1 r_1\left(\boldsymbol{P}^{i,k}_n - \boldsymbol{X}^{i,k}_n\right) + c_2 r_2\left(\boldsymbol{G}^{i,k} - \boldsymbol{X}^{i,k}_n\right) \tag{12}$$

$$\boldsymbol{X}^{i,k+1}_n = \boldsymbol{X}^{i,k}_n + \boldsymbol{V}^{i,k+1}_n \tag{13}$$

where ω is the inertia weight. c_1 and c_2 are the accelerating factor. r_1 and r_2 are weight factor whose ranges are set as [0, 1]. k represents the current iteration number. As long as it reaches the preset value or the current fitness is smaller the threshold value, the circulation will stop and output the optimal position vector.

C. STEP THREE: RECONSTRUCTION AND PROJECTING

In step three, we reconstruct the measured rail profiles employing the position vector obtained in step two as the final light plane parameters from (4), and project them onto the auxiliary plane established in step one. No matter whether there is random vibration in the lase projector, the projecting is able to yield a rectified and useful rail profile either from the normal profile or from the distorted one. These works are therefore simple and effective.

Figure 5 exhibits a case visual showing the rectifying process. In Fig. 5(a), neither the rail head inner nor the rail foot of the distorted profiles shows any overlap with the standard one, which is caused by the random vibration. The rectified profile is given in Fig. 5(b). Except for the worn head, the rectified profile is aligned well with the standard one, which verifies the validity of the projecting.

IV. EXPERIMENTS AND DISCUSSION

In this section, comprehensive experiments are presented for the evaluation of our method. Firstly, the performance of step two, self-calibration, was assessed for different rail types and poses. Then, the rectifying presented in step three was compared with the previous works, whose validity and repeatability have been tested as well. Finally, we discussed the calculated load.

A. PERFORMANCE ASSESSMENT ON SELF-CALIBRATION

1) ASSESSMENT WITH TWO RAIL TYPES

In this assessment, type 60 and type 50, two kinds of rail widely used in china, were served as the test object to assess the effectiveness and adaptability of the proposed calibration

TABLE 1. Parameters of light planes 1 and 2 calibrated via different ways.

Methods	Light plane 1	Light plane 2	Average times
1D target-based	$z_c = 1.9841x_c$-$0.2028y_c + 957.7954$	$z_c = 1.8756x_c$-$0.1713y_c + 917.6481$	329 ms
Self-calibration on type 60	$z_c = 1.9816x_c$-$0.2054y_c + 956.5471$	$z_c = 1.8969x_c$-$0.1624y_c + 916.5837$	161 ms
Self-calibration on type 50	$z_c = 1.9794x_c$-$0.2033y_c + 956.6998$	$z_c = 1.9166x_c$-$0.1695y_c + 916.9237$	155 ms

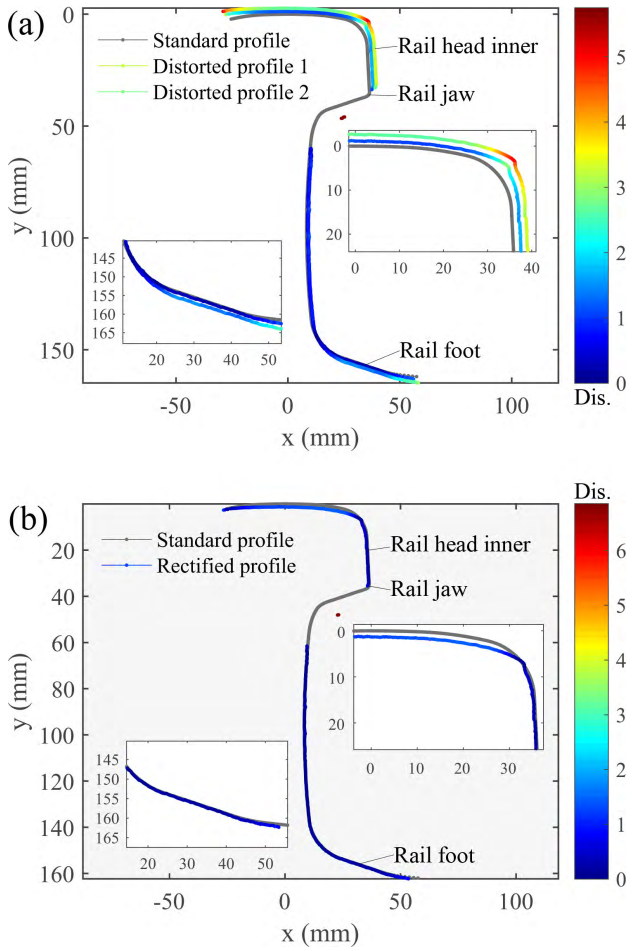

FIGURE 5. An example of reconstruction and projecting rectification. (a) The standard profile and the distorted profiles. (b) The standard profile and the rectified one.

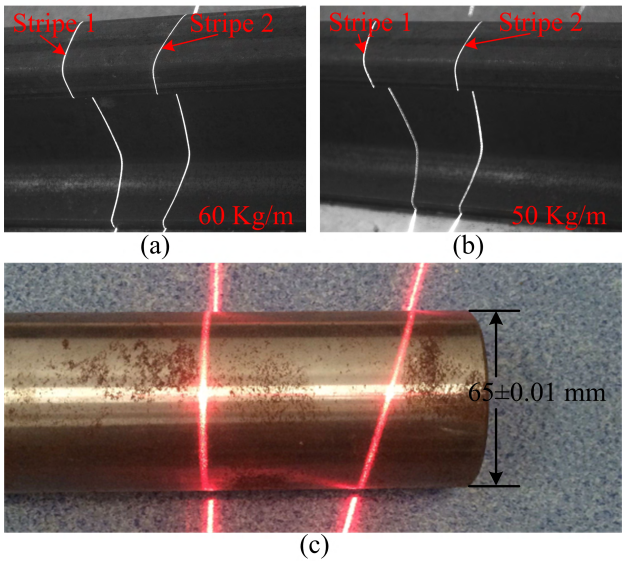

FIGURE 6. Several cases for the performance assessment on self-calibration proposed in subsection III-B. (a) Assessment with type 60. (b) Assessment with type 50. (c) Accuracy assessment with a standard cylinder.

scheme. The type m means the weight of rail with length of one meter is m kilogram. Respectively, 50 scene images were repeatedly taken from two rail specimens. As shown in Figs. 6(a) and 6(b), the light planes 1 and 2 intersect the rail yielding the stripes 1 and 2. According to step two in subsection III-B, we calculated their parameters with respect to the camera coordinate frame, which are then compared against these determined by 1D target-based calibration, a well-established approach proposed in [34]. Table I lists their calibration results.

Table 1 exhibits that all the parameters obtained neither on type 60 nor 50 show any significant deviation with those obtained by Wei *et al.* [34], from which we can verify the feasibility of the presented self-calibration on various types of rail. Furthermore, the average time of our procedure is nearly half of this needed by 1D target-based calibration. It means the computational speed of ours is faster. The 1D target-based calibration based on the nonlinear optimization requires complex iterations, and depends on a precise gauge with three feature points. By contrast, our on-line self-calibration profits from the parallelity characteristic of rail and PSM, and needs only one image with two stripes. Clearly, this scheme owns so attractive merit such as flexibility and practicality that it exhibits more fitness for the dynamic inspection.

To make further investigation on the accuracy of the parameters in Table 1, a steel cylinder whose cross-sectional diameter is 65 $\pm$ 0.01 millimeters was utilized in regards to this assessment, as demonstrated in Fig. 6(c). Its cross profile and diameter were fitted using the calibrated double-line SLV. Twenty fitted diameters at several positions were calculated, and their statistics such as root mean squared error (RMSE) [35], [36] is analyzed and compared. Specifically, RMSE from the setup calibrated by Wei *et al.* [34] is 0.064 mm. Relatively, Ours are relatively lower, at 0.055 and 0.060 mm, respectively.

2) ASSESSMENT WITH DIFFERENT POSTURES

Relative postures of double-line structured-light employed above are constant. In this subsection, a series of double-line structured-lights with three different postures were adopted

TABLE 2. Results of wear inspection for type 60 rail.

	True wears (mm)		Wears acquired by CH (mm)				Wears acquired by Sun (mm)				Wears acquired by our method (mm)			
No.	Vw	Hw	Vw	Error	Hw	Error	Vw	Error	Hw	Error	Vw	Error	Hw	Error
1	1.38	-0.41	0.89	0.49	-0.54	0.13	1.19	0.19	-0.47	0.06	1.37	0.01	-0.44	0.03
2	1.14	-0.21	1.02	0.12	-0.59	0.38	1.04	0.1	-0.32	0.11	1.06	0.08	-0.3	0.09
3	1.24	-0.34	1.17	0.07	-0.48	0.14	1.21	0.03	-0.42	0.08	1.21	0.03	-0.42	0.08
4	1.3	-0.29	1.1	0.2	-0.51	0.22	1.12	0.18	-0.38	0.09	1.25	0.05	-0.4	0.11
5	1.05	-0.4	0.85	0.2	-0.42	0.02	0.99	0.06	-0.55	0.15	1.02	0.03	-0.46	0.06
6	1.22	-0.3	0.96	0.26	-0.39	0.09	1.12	0.1	-0.44	0.14	1.18	0.04	-0.37	0.07
7	1.27	-0.29	0.89	0.38	-0.41	0.12	1.07	0.2	-0.49	0.2	1.17	0.1	-0.35	0.06
8	1.35	-0.41	1.1	0.25	-0.5	0.09	1.19	0.16	-0.5	0.09	1.05	0.3	-0.57	0.16
9	1.1	-0.28	0.97	0.13	-0.44	0.16	1.01	0.09	-0.33	0.05	1.05	0.05	-0.36	0.08
10	1.19	-0.32	1.04	0.15	-0.57	0.25	1.09	0.1	-0.45	0.13	1.08	0.11	-0.39	0.07
RMSE (mm)			-	0.255	-	0.186	-	0.132	-	0.118	-	0.112	-	0.087
MAPE (%)			-	18.03	-	56.33	-	9.69	-	35.51	-	6.40	-	26.01

in the performance assessment. Again, we analyzed the self-calibration accuracy from RMSE. Specifically, the RMSE of twenty fitted diameters with poses 1, 2 and 3 are respectively 0.054, 0.056 and 0.060 mm. All of them are superior to 0.064 mm acquired by Wei *et al.* [34]. These comparisons and inspection results indicate the ideal result of our on-line self-calibration scheme.

B. PERFORMANCE ASSESSMENT ON DISTORTION RECTIFYING

The main purpose in our article is to exploit an effective distortion rectifying scheme for the dynamic inspection of track wear from double-line SLV. The performance of our distortion rectifying method was assessed by a series of actual experiments. In these experiments, the horizontal and vertical wears are taken as the assessment criterion. Referring to the railway maintenance rules, the wear on the position far from the top of rail by 16 mm is referred as to the horizontal wear, and the wear on the position locating at the one third width of rail head surface is referred as to the vertical wear. By analyzing the deviations on the corresponding places from the inspected rail profile to the standard one, two kinds of wear are calculated, respectively. Similar to subsection IV-A, assessment with two different rails was performed. Herein, ten distorted profiles were taken respectively from different locations of the type 60 and type 50 rails, and were aligned with the standard profile to calculate rail wear. Their true values were obtained manually by rail slide gauge. For comparison, the convex hull (CH) [16] and the procedure presented in [18] were employed as the other way to inspect wear. The RMSE and mean absolute percentage error (MAPE) with respect to the true value were analyzed, and listed in Tables 2 and 3, respectively. Note that abbreviations Vw and Hw denote the vertical wear and horizontal wear, respectively.

In Table 2, it can be found that the rail wears inspected by the proposed method are the nearest ones to the true value. Superior to the data acquired by CH and Sun, the RMSE of Vw and Hw generated from our scheme decline to 0.112 and 0.087 mm, respectively. Moreover, their MAPE are small as well, respectively at 6.40% and 26.01%. From Table 3, the similar superiority would also be seen due to the commendable RMSE and MAPE, which indicates the excellent performance of our method on type 50 rail. Hence, the proposed distortion rectifying would be available for various rail types, given that there are two parallel lines detected from the waist and foot of rail track.

The excellent performance of our rectifying can be comprehended from several influencing factors.

Firstly, profiting from parallelity constraint, the auxiliary projecting plane is established accurately utilizing the intrinsic camera parameters. It is therefore stabilized and robust to the dynamic behaviors on the light planes. Compared to the projecting plane established in [18], which is based on the offline calibrated parallel-line SLV, ours owns a higher reliability.

Secondly, provided the reliable auxiliary plane and PSM, the parameters of light planes are calculated autonomously via the proposed self-calibration procedure. They are also very robust with respect to the assembling deviation and vibrancy in laser projectors, which guarantees the correct reconstruction of the rail profile.

Thirdly, CH based distortion rectifying [16] concentrates on the establishment of the corresponding points from the distorted profile to standard one. Yet, the quantity and the distribution of their points is distinguishing, which may lead to the unreliable correspondences. Our distortion rectifying based on the coordinate projecting does not depend on the standard profile, it owns accuracy superior to CH as a result.

C. REPEATABILITY TEST OF WEAR INSPECTION

1) STATIC REPEATABILITY TEST

The static repeatability reflects the consistency of repetitive inspections on one measuring position. Herein, we randomly

TABLE 3. Results of wear inspection for type 50 rail.

	True wears (mm)		Wears acquired by CH (mm)				Wears acquired by Sun (mm)				Wears acquired by our method (mm)			
No.	Vw	Hw	Vw	Error	Hw	Error	Vw	Error	Hw	Error	Vw	Error	Hw	Error
1	2.01	-0.29	2.32	-0.31	-0.33	0.04	2.18	-0.17	-0.51	0.22	2.07	-0.06	-0.44	0.15
2	2.34	-0.39	2.22	0.12	-0.52	0.13	2.14	0.2	-0.48	0.09	2.24	0.1	-0.37	-0.02
3	2.29	-0.41	2.34	-0.05	-0.47	0.06	2.16	0.13	-0.48	0.07	2.21	0.08	-0.34	-0.07
4	2.38	-0.22	2.01	0.37	-0.4	0.18	2.18	0.2	-0.39	0.17	2.45	-0.07	-0.27	0.05
5	2.05	-0.29	2.15	-0.1	-0.48	0.19	2.09	-0.04	-0.4	0.11	2.1	-0.05	-0.27	-0.02
6	2.03	-0.38	2.27	-0.24	-0.47	0.09	2.12	-0.09	-0.45	0.07	2.17	-0.14	-0.48	0.1
7	2.2	-0.44	2.08	0.12	-0.25	-0.19	2.09	0.11	-0.45	0.01	2.18	0.02	-0.5	0.06
8	2.14	-0.47	2.29	-0.15	-0.27	-0.2	2.18	-0.04	-0.45	-0.02	2.15	-0.01	-0.38	-0.09
9	2.32	-0.3	2.41	-0.09	-0.39	0.09	2.13	0.19	-0.4	0.1	2.26	0.06	-0.26	-0.04
10	2.1	-0.35	2.25	-0.15	-0.47	0.12	2.2	-0.1	-0.41	0.06	2.24	-0.14	-0.47	0.12
RMSE (mm)			-	0.196	-	0.140	-	0.139	-	0.110	-	0.084	-	0.083
MAPE (%)			-	7.85	-	38.28	-	5.73	-	33.66	-	3.37	-	21.23

TABLE 4. Statistics of repeatability error on wears inspected multiply.

	Statistics of repeatability error for multiple inspections	
Positions	ΔD_{v}(mm)	ΔD_{h}(mm)
1	0.011	0.010
2	0.012	0.012
3	0.013	0.016

chose three inspecting points on a type 60 rail, and moved the light projector 1 for the intersection of the light plane 1 with three measuring positions at a constant angle. In each position, the Vw and Hw were inspected repeatedly for this test. The wear curves are presented in Figs. 7(a) and 7(b), respectively. It is clear that neither the Vw nor Hw shows any significant change in their values, just fluctuates in a very small range. Concretely, the Vw inspected in positions 1, 2 and 3 undulates respectively nearby 1.18, 1.27 and 1.16 mm, and the Hw undulates respectively nearby −0.46, −0.48 and −0.56 mm. Their fluctuation ranges are no more than 0.05 mm, which indicates the high repeatability of the proposed method for the multiple inspections.

To further state the static repeatability, we calculated repeatability error statistics of inspected wears in each position and reported the quantitative analysis as listed in Table 4. The symbols ΔD_{v} and ΔD_{h} represent the standard deviations of inspected wears. For different positions, all of them are small enough, achieving minor repeatability errors no more than 0.02 mm. These analyses also confirm the good stability of our method.

2) DYNAMIC REPEATABILITY TEST

As stated in [10], the inspected rail profile would suffer from different equal-scale stretches as the light plane intersects the rail at different angles. Dynamic repeatability means the inspection consistency for diverse equal-scale stretches on the distorted profile. It is tested by three inspection experiments,

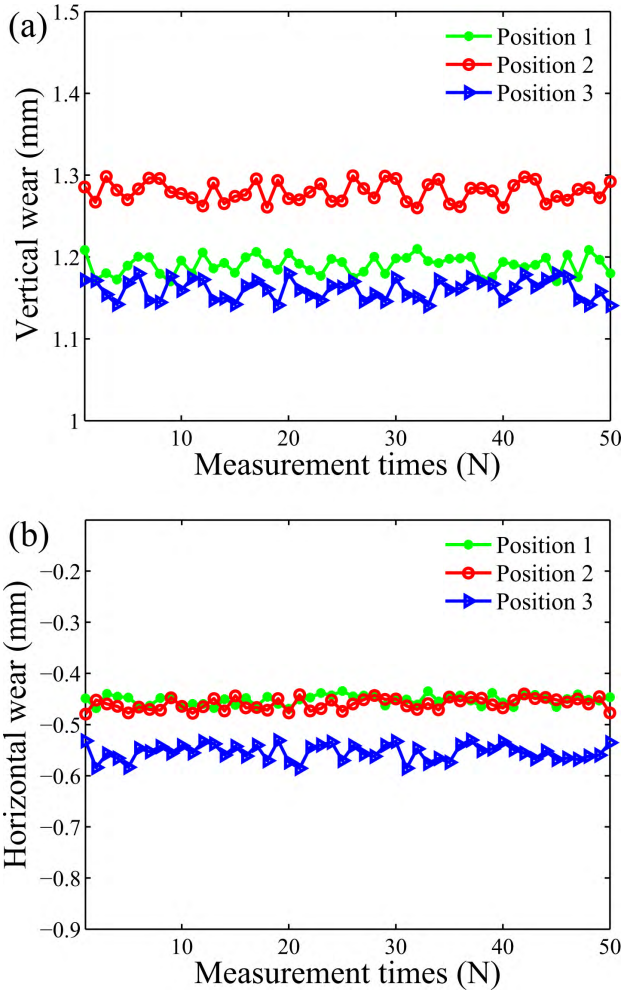

FIGURE 7. The wears inspected from three positions. (a) Vertical wear. (b) Horizontal wear.

for which light plane 1 was adjusted for different intersection angles with the rail. We inspected the wear every one meter along a type 60 rail for 50 meters. The results are shown

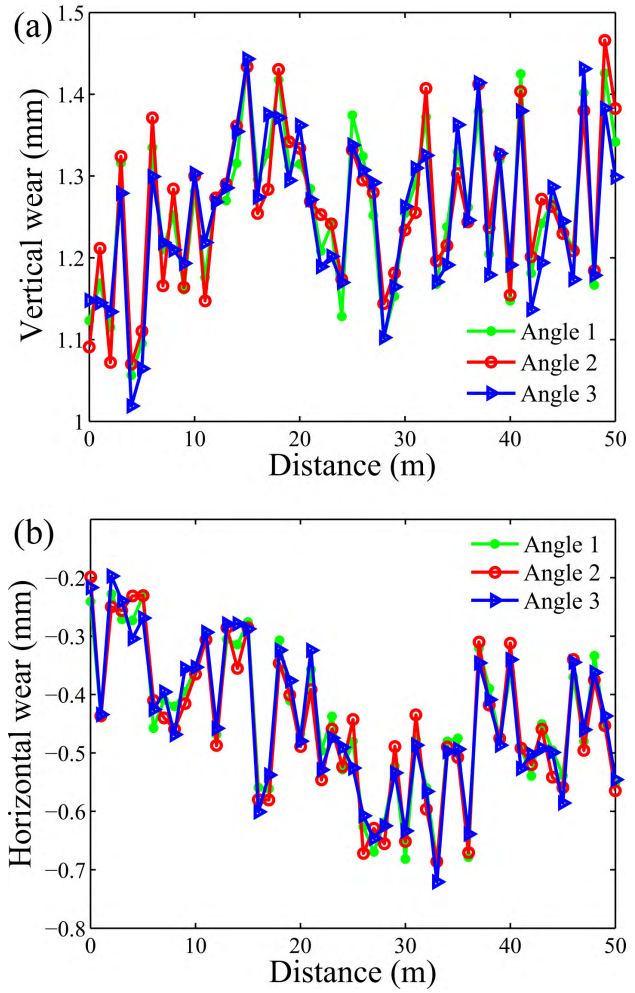

FIGURE 8. The wears inspected with diverse angles. (a) Vertical wear. (b) Horizontal wear.

in Fig. 8. Clearly, the wear curves exhibit the similar tendency in spite of the different equal-scale stretches, and are basically in line with each others within a same inspection interval. The survey results indicate that the proposed procedure owns high repeatability even if there are distortions in different degrees on the measured profiles.

Again, the repeatability error was reported to evaluate the dynamic repeatability quantitatively. Table 5 lists the repeatability error statistics of inspected wears for the diverse angles, where symbols ΔM_{v} and ΔM_{h} respectively represent the averages of standard deviations on the inspected Vw and Hw. Clearly, both of them are small enough, achieving minor repeatability errors no more than 0.03 mm. The above data manifest the strong stability and repeatability with respect to the different profiles distorted in different degrees. From Fig. 8 and Table 5, we are aware of that our scheme possesses desired dynamic repeatability, which can be explained by two following facts.

First, combining the previously calibrated camera parameters, the proposed on-line self-calibration of the double-line SLV ensures the accurate reconstruction of the inspected rail profile. It is therefore immune to the variation in the pose of the camera and projector.

TABLE 5. Statistics of repeatability error on wears inspected from diverse angles.

Statistics of repeatability error on different angles	
ΔM_{v}(mm)	ΔM_{h}(mm)
0.024	0.020

Second, the projecting based distortion rectifying is also not subject to the degree of the distortion, which further promotes our repeatability and stability.

D. ANALYSIS OF COMPUTATIONAL LOAD

On the basis of the procedure, we analyze the computational load for the three steps, i.e., establishment of the auxiliary plane, self-calibration of the structured-light and projecting. In step one, the auxiliary plane is established from one image with two stripes of the rail profile. The time complexity is $O(1)$. There are two parts in step two. First, the rail profile is reconstructed using SLV model, and is projected onto the auxiliary projecting plane. Their time complexity is $O(n)$ in total. Then, the PSM errors of triple matching primitives are calculated and minimized by PSO. Its time complexity is $O(n \times N \times G)$. Here, n denotes the quantity of the mapping primitives. Variables N and G are number of times for iteration and the number of particles for one swarm, respectively. Accordingly, time complexity in step two is $O(n \times N \times G)$. In step three, the reconstructed profile is projected onto the established auxiliary plane for the distortion rectifying, whose time complexity is $O(n)$. Overall, our time complexity would be analyzed as $(O(1) + O(n \times N \times G) + O(n))$, and is equivalent to $O(n \times N \times G)$.

Furthermore, a timing experiment was also performed to test the mean time consuming for the wear inspection. The program was run on 100 inspecting images, which contain 200 distorted profiles in all. The mean temporal demand on once inspection is approximately 175 ms. According to the rail maintenance rule, the interval for each wear inspections is commonly defined to 0.25 m. Consequently, it is able to be deduced that our mean inspection speed is about 5.14 km/h, which is faster than the maximum velocity of the rail maintenance vehicle.

V. CONCLUSION

In this paper, a valid rail wear inspection technique used in the SLV system is proposed to handle the distorted profile caused by the dynamic behaviors. It mainly involves three steps: establishment of an auxiliary plane, on-line self-calibration, and projecting rectifying. The proposed procedure was evaluated by a set of experiments. As a key step, the self-calibration has been assessed with different rail types and structured-light poses. The results of performance assessment and comparison indicate that it performs as well as the target-based calibration even when the additional calibration

gauge is unavailable. The proposed rectifying method was also assessed by comparing against other well-established schemes, and its repeatability and computational load were investigated. The survey results show that our method performs significantly better in regards to the dynamic inspection of rail wear, and owns high static repeatability together with dynamic repeatability. At the same time, this method is able to meet the speed requirement by the rail maintenance vehicle.

ACKNOWLEDGMENT

The authors would like to thank the editors and the anonymous reviewers for their time and effort in reviewing this paper.

REFERENCES

[1] J. Molleda *et al.*, "A profile measurement system for rail quality assessment during manufacturing," *IEEE Trans. Ind. Appl.*, vol. 52, no. 3, pp. 2684–2692, May/Jun. 2016.

[2] P. Giri and S. Kharkovsky, "Detection of surface crack in concrete using measurement technique with laser displacement sensor," *IEEE Trans. Instrum. Meas.*, vol. 65, no. 8, pp. 1951–1953, Aug. 2016.

[3] *The Ministry of Railway for the People's Republic of China 2012 Railway Transportation 2006-146: Railway Maintenance Rules*, China Railway, Beijing, China, 2012.

[4] R. Chen, J. Xu, S. Zhang, H. Chen, Y. Guan, and K. Chen, "A self-recalibration method based on scale-invariant registration for structured light measurement systems," *Opt. Lasers Eng.*, vol. 88, pp. 75–81, Jan. 2017.

[5] M. Vo, S. G. Narasimhan, and Y. Sheikh, "Texture illumination separation for single-shot structured light reconstruction," *IEEE Trans. Pattern Anal. Mach. Intell.*, vol. 38, no. 2, pp. 390–404, Feb. 2016.

[6] S. R. Fanello *et al.*, "HyperDepth: Learning depth from structured light without matching," in *Proc. IEEE Conf. Comput. Vis. Pattern Recognit. (CVPR)*, Jun. 2016, pp. 5441–5450.

[7] P. Zhou, K. Xu, and D. Wang, "Rail profile measurement based on line-structured light vision," *IEEE Access*, vol. 6, pp. 16423–16431, 2018.

[8] G. Panahandeh, M. Jansson, and P. Händel, "Calibration of an IMU-camera cluster using planar mirror reflection and its observability analysis," *IEEE Trans. Instrum. Meas.*, vol. 64, no. 1, pp. 75–88, Jan. 2015.

[9] K. Tamura, R. Choi, and Y. Aoki, "Unconstrained and calibration-free gaze estimation in a room-scale area using a monocular camera," *IEEE Access*, vol. 6, pp. 10896–10908, 2018.

[10] H. Liu, Y. Li, Z. Ma, and C. Wang, "Recognition and calibration of rail profile under affine-distortion-based point set mapping," *IEEE Trans. Instrum. Meas.*, vol. 66, no. 1, pp. 131–140, Jan. 2017.

[11] D. Zhan, L. Yu, J. Xiao, and T. Chen, "Study on high-accuracy vision measurement approach for dynamic inspection of full cross-sectional rail profile," *J. China Railway Soc.*, vol. 37, no. 9, pp. 96–106, 2015.

[12] D. Zhan, L. Yu, J. Xiao, and M. Lu, "Study on dynamic matching algorithm in inspection of full cross-sectional rail profile," *J. China Railway Soc.*, vol. 37, no. 5, pp. 71–77, 2015.

[13] B. Jian and B. C. Vemuri, "Robust point set registration using Gaussian mixture models," *IEEE Trans. Pattern Anal. Mach. Intell.*, vol. 33, no. 8, pp. 1633–1645, Aug. 2011.

[14] H. Hontani, T. Matsuno, and Y. Sawada, "Robust nonrigid ICP using outlier-sparsity regularization," in *Proc. IEEE Conf. Comput. Vis. Pattern Recognit. (CVPR)*, Jun. 2012, pp. 174–181.

[15] X. Huang, B. Wang, and L. Zhang, "A new scheme for extraction of affine invariant descriptor and affine motion estimation based on independent component analysis," *Pattern Recognit. Lett.*, vol. 26, no. 9, pp. 1244–1255, 2005.

[16] Z. Yang and F. S. Cohen, "Image registration and object recognition using affine invariants and convex hulls," *IEEE Trans. Image Process.*, vol. 8, no. 7, pp. 934–946, Jul. 1999.

[17] C. Wang, Z. Ma, Y. Li, J. Zeng, T. Jin, and H. Liu, "Deviation rectification for dynamic measurement of rail wear based on coordinate sets projection," *Meas. Sci. Technol.*, vol. 28, no. 10, p. 105203, 2017.

[18] J. Sun, Z. Liu, Y. Zhao, Q. Liu, and G. Zhang, "Motion deviation rectifying method of dynamically measuring rail wear based on multi-line structured-light vision," *Opt. Laser Technol.*, vol. 50, pp. 25–32, Sep. 2013.

[19] Z. Liu, J. H. Sun, H. Wang, and G. J. Zhang, "Simple and fast rail wear measurement method based on structured light," *Opt. Lasers Eng.*, vol. 49, no. 11, pp. 1343–1351, Nov. 2011.

[20] C. Wang, Y. Li, Z. Ma, J. Zeng, T. Jin, and H. Liu, "Distortion rectifying for dynamically measuring rail profile based on self-calibration of multiline structured light," *IEEE Trans. Instrum. Meas.*, vol. 67, no. 3, pp. 678–689, Mar. 2018.

[21] P. Kiddee, Z. Fang, and M. Tan, "A practical and intuitive calibration technique for cross-line structured light," *Optik*, vol. 127, no. 20, pp. 9582–9602, 2016.

[22] P. Kiddee, Z. Fang, and M. Tan, "An automated weld seam tracking system for thick plate using cross mark structured light," *Int. J. Adv. Manuf. Technol.*, vol. 87, nos. 9–12, pp. 3589–3603, Apr. 2016.

[23] Y. Li, H. Trinh, N. Haas, C. Otto, and S. Pankanti, "Rail component detection, optimization, and assessment for automatic rail track inspection," *IEEE Trans. Intell. Transp. Syst.*, vol. 15, no. 2, pp. 760–770, Apr. 2014.

[24] J.-H. Sun, H. Wang, Z. Liu, and G. J. Zhang, "Rapid extraction algorithm of laser stripe center in rail wear dynamic measurement," *Opt. Precis. Eng.*, vol. 19, no. 6, pp. 690–696, 2011.

[25] F. Bruno, G. Bianco, M. Muzzupappa, S. Barone, and A. Razionale, "Experimentation of structured light and stereo vision for underwater 3D reconstruction," *ISPRS J. Photogramm. Remote Sens.*, vol. 66, no. 4, pp. 508–518, 2011.

[26] J. Salvi, S. Fernandez, T. Pribanic, and X. Llado, "A state of the art in structured light patterns for surface profilometry," *Pattern Recognit.*, vol. 43, no. 8, pp. 2666–2680, Aug. 2010.

[27] Z. Zhang, "A flexible new technique for camera calibration," *IEEE Trans. Pattern Anal. Mach. Intell.*, vol. 22, no. 11, pp. 1330–1334, Nov. 2000.

[28] B. A. Jasani, S.-K. Lam, P. K. Meher, and M. Wu, "Threshold-guided design and optimization for harris corner detector architecture," *IEEE Trans. Circuits Syst. Video Technol.*, to be published, doi: 10.1109/TCSVT.2017.2757998.

[29] C. Harris and M. Stephens, "A combined corner and edge detector," in *Proc. Alvey Vision Conf.*, 1988, pp. 147–151.

[30] Y. F. Li and S. Y. Chen, "Automatic recalibration of an active structured light vision system," *IEEE Trans. Robot. Autom.*, vol. 19, no. 2, pp. 259–268, Apr. 2003.

[31] B. Yi, Y. Yang, Q. Yi, W. Dai, and X. Li, "Novel method for rail wear inspection based on the sparse iterative closest point method," *Meas. Sci. Technol.*, vol. 28, no. 12, p. 125201, 2017.

[32] O. Sandre-Hernandez, R. Morales-Caporal, J. Rangel-Magdaleno, H. Peregrina-Barreto, and J. N. Hernandez-Perez, "Parameter identification of PMSMs using experimental measurements and a PSO algorithm," *IEEE Trans. Instrum. Meas.*, vol. 64, no. 8, pp. 2146–2154, Aug. 2015.

[33] E. Zhang, L. Hou, C. Shen, Y. Shi, and Y. Zhang, "Sound quality prediction of vehicle interior noise and mathematical modeling using a back propagation neural network (BPNN) based on particle swarm optimization (PSO)," *Meas. Sci. Technol.*, vol. 27, no. 1, p. 015801, 2016.

[34] Z. Wei, L. Cao, and G. Zhang, "A novel 1D target-based calibration method with unknown orientation for structured light vision sensor," *Opt. Laser Technol.*, vol. 42, no. 4, pp. 570–574, 2010.

[35] X. Deng, Z. Tang, L. T. Yang, M. Lin, and B. Wang, "Confident information coverage hole healing in hybrid industrial wireless sensor networks," *IEEE Trans. Ind. Informat.*, vol. 14, no. 5, pp. 2220–2229, May 2018.

[36] L. Yi, X. Deng, M. Wang, D. Ding, and Y. Wang, "Localized confident information coverage hole detection in Internet of Things for radioactive pollution monitoring," *IEEE Access*, vol. 5, pp. 18665–18674, 2017.

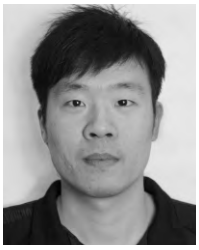

CHAO WANG received the B.Sc. degree in electronic information engineering from Hunan Normal University, Changsha, China, in 2008. He is currently pursuing the Ph.D. degree with the College of Electrical and Information Engineering, Hunan University. His current research interests include machine vision, railway inspection, and signal processing.

HONGLI LIU received the B.Sc. degree in electrical engineering and the Ph.D. degree in control theory and engineering from Hunan University, China, in 1985 and 2000, respectively. He is currently a Professor with the College of Electrical and Information Engineering, Hunan University. His research interests include intelligent information processing and transmission technology.

ZIJI MA received the B.Sc. degree in electronic information engineering from Hunan University, China, in 2001, and the Ph.D. degree in information science from the Nara Institute of Science and Technology, Nara, Japan, in 2012. He is currently an Assistant Professor with Hunan University. His research interests include machine vision, railway inspection, and signal processing.

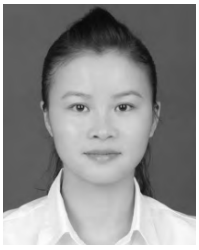

JIUZHEN ZENG received the B.Sc. degree in electronic information engineering from Hunan Normal University, China, in 2008. She is currently an Assistant Professor with the University of South China, Hengyang, China. Her current research interests include machine vision and signal processing.